Hao Chen and Hongping Xiang*

First low-spin carbodiimide, $Fe_2(NCN)_3$, predicted from first-principles investigations

https://doi.org/10.1515/znb-2021-0128
Received August 31, 2021; accepted September 8, 2021;
published online September 21, 2021

Abstract: The structural stability and physical properties of the Fe(III) carbodiimide $Fe_2(NCN)_3$ were studied by use of density functional theory. The results indicate that $Fe_2(NCN)_3$ (space group $R\bar{3}c$) is stable both thermodynamically and mechanically. The electronic structure in combination with the phonon dispersion relations suggest that the title compound should be ferromagnetic and half-metallic, and that the Fe^{3+} ions are in the low-spin state.

Keywords: density functional theory; $Fe_2(NCN)_3$; transition metal carbodiimide.

Dedicated to Professor Richard Dronskowski on the Occasion of his 60th Birthday

1 Introduction

Recently, a new class of 3*d* transition metal carbodiimides has attracted much attention due to their potential functional properties such as magnetic behavior [1–10] and promising anode materials for both Li- and Na-ion batteries [11–17]. The doubly charged complex anion $(NCN)^{2-}$ displays a pseudochalcogen character [18] and exists in two forms, a linear $[N{=}C{=}N]^{2-}$ with two N=C double bonds so-called carbodiimide and a less symmetrical $[N{-}C{\equiv}N]^{2-}$ named cyanamide. The symmetric carbodiimides $[N{=}C{=}N]^{2-}$ appear to be an ideal anion for the formation of transition metal magnetic frameworks [19].

Most 3*d* transition metal(II) carbodiimides exhibit some similarities in crystal structures as compared to their corresponding monoxides. MnNCN, which adopts a hexagonal structure with space group $R\bar{3}m$, is an optically transparent, green-colored antiferromagnetic insulator [1, 20]. In experimental and theoretical studies it has been found that MnNCN has a larger degree of covalent bonding than MnO and a narrower indirect charge transfer-type electronic band gap [20]. Crystals of the compounds FeNCN, CoNCN, and NiNCN are hexagonal systems with the space group $P6_3/mmc$ [2, 19], and represent a uniform group of high-spin antiferromagnetic, optically transparent, colored insulators with absorption lines in the visible spectrum. The EHCF numerical modeling suggested a mechanism of the *d*–*d* intra-shell transitions for their visible absorption spectra [21], which is different from the charge transfer-type found in MnNCN [20]. All three compounds are type-II antiferromagnetic, i.e. intralayer ferromagnetic and interlayer antiferromagnetic, similar to their corresponding monoxides [9]. CuNCN crystallizes in the orthorhombic structure with the space group *Cmcm*, showing some crystallographic similarities with CuO and high temperature superconductors (HTSCs) [3, 7]. However, CuNCN shows a nonmagnetic behavior even at low temperature as demonstrated by magnetic measurements, quite different from the antiferromagnetism of CuO and that of HTSCs. Nevertheless, a structural anomalous change at low temperature was observed for CuNCN from high-resolution neutron powder diffraction data, hinting at a changing magnetic behavior [8].

Compared to the well-studied 3*d* transition metal (M, II) carbodiimides, up to now for M(III) carbodiimides, only $Cr_2(NCN)_3$ has been successfully synthesized [4]. $Cr_2(NCN)_3$ is a green ferromagnetic material, and displays a crystallographic structure similar to that of the oxide Cr_2O_3 with the space group of $R\bar{3}c$. The ferromagnetic behavior is quite different from the antiferromagnetism of Cr_2O_3 and of all other 3*d* transition metal (M, II) carbodiimides. A neutron diffraction study of $Cr_2(NCN)_3$ has demonstrated a magnetic two-step transition scenario over an unusual wide temperature range [22], from 3D paramagnetism to a lower dimensional ferromagnetic ordering (a possible 2D-ferromagnetic ordering) below T_{LD} = 166 K, and then to a complete 3D-ferromagnetic ordering below T_c = 114 K. The electronic structures based on density functional theory calculations suggest that $Cr_2(NCN)_3$ is an intermediate between a charge transfer case and a Mott-Hubbard insulator, similar to the related Cr_2O_3 [4].

***Corresponding author: Hongping Xiang,** School of Materials Science and Engineering, Tongji University, 4800 Cao'an Road, Shanghai 201804, P. R. China, E-mail: xianghp@tongji.edu.cn
Hao Chen, School of Materials Science and Engineering, Tongji University, 4800 Cao'an Road, Shanghai 201804, P. R. China

Its rich physical properties, potential applications, as well as its importance in the study of magnetic mechanisms, has motivated us to investigate the hypothetical 3*d* transition metal (III) carbodiimide, $Fe_2(NCN)_3$. In this study, we first examine the structural stability both thermodynamically and mechanically, and then study the electronic and magnetic properties by use of density functional theory. It is interesting to find that $Fe_2(NCN)_3$ was predicted to be the first low-spin carbodiimide.

2 Theoretical calculations

The periodic density functional theory [23, 24] calculations were carried out by means of the plane-wave pseudopotential Vienna ab initio Simulation Package (VASP) [25–27]. The generalized gradient approximation as formulated by Perdew, Burke and Ernzerhof (GGA-PBE) was employed for the exchange correlation-functional [28]. The projector-augmented wave (PAW) method which was proposed by Blöchl [29] and implemented by Kresse and Joubert [30] was used, with a cutoff energy of 800 eV. $7 \times 7 \times 7$ **k**-points were used to sample the complete Brillouin zone, and a $9 \times 9 \times 9$ **k**-points grid was used to calculate the density-of-states. Brillouin zone integrations were performed with the tetrahedron method and Blöchl's corrections [31]. The PAW pseudopotentials are $3d^6 4s^2$ for Fe, $2s^2 2p^3$ for N, and $2s^2 2p^2$ for C. Electron–electron Coulomb interactions for the Fe atoms in combination with the self-interaction correction were considered in the rotationally invariant method (GGA + *U*) with an effective Hubbard parameter $U_{\text{eff}} = U - J$ [32, 33]. The calculations were started with a non-magnetic ground state, and then spin polarization was employed. Finally, a finite *U* value was allowed for.

Density-functional perturbation theory (DFPT) [34, 35] in VASP coupled with the analysis program Phonopy [36] was used to calculate the phonon frequencies of $Fe_2(NCN)_3$. The unit cell including 66 atoms was used to calculate the force constants. 101 **k**-points were used to sample each segment of the band paths in order to obtain phonon dispersion relations.

A hexagonal crystal structure with space group $R\bar{3}c$ was chosen for $Fe_2(NCN)_3$, taken from $Cr_2(NCN)_3$ [4] and α-Fe_2O_3 [37]. The 3*d* transition metal compounds with the $[N{=}C{=}N]^{2-}$ ligand have been proven to show similar crystal structures as the corresponding oxides such as in the case of $Cr_2(NCN)_3$ and Cr_2O_3 [4]. The initial crystal structure was optimized by relaxing of all lattice parameters and the positions of Fe, C, and N simultaneously until self-consistency was achieved.

3 Results and discussion

The optimized crystal structures of $Fe_2(NCN)_3$ in space group $R\bar{3}c$ is displayed in Figure 1. The calculated lattice parameters of the unit cell (left in Figure 1) are $a = 5.1865$, $c = 27.7013$ Å, $V = 645.321$ Å^3, and $Z = 6$. The Fe^{3+} ions are on the Wyckoff position 12*c* with $z = 0.1661$, forming sheets of cations parallel to the *ab* face with a Fe–Fe distance of 2.995 Å. Each Fe^{3+} ion is coordinated by six nitrogen atoms on 36*f* with $x = 0.3282$, $y = 0.0391$, and $z = 0.1271$, corresponding to a distorted FeN_6 octahedron with Fe–N bond lengths of 1.992 and 1.938 Å (three of each). The NCN^{2-} anion, which is nearly linear with a 176.446° angle of N–C–N, experiences a distorted tetrahedral coordination by the Fe ions, and almost coincides with the *c* axis. This anionic unit adopts the symmetrical carbodiimide shape with C–N 1.230 Å. Obviously, $Fe_2(NCN)_3$ features a structure with alternating layers Fe^{3+} and NCN^{2-} ions along the *c* axis (Figure 1; left). Nonetheless, the packing of the metal layers is not dense because each atom is surrounded by only three neighboring metal atoms.

The chemical reaction energy was obtained as the total energy of the product minus the total energy of the

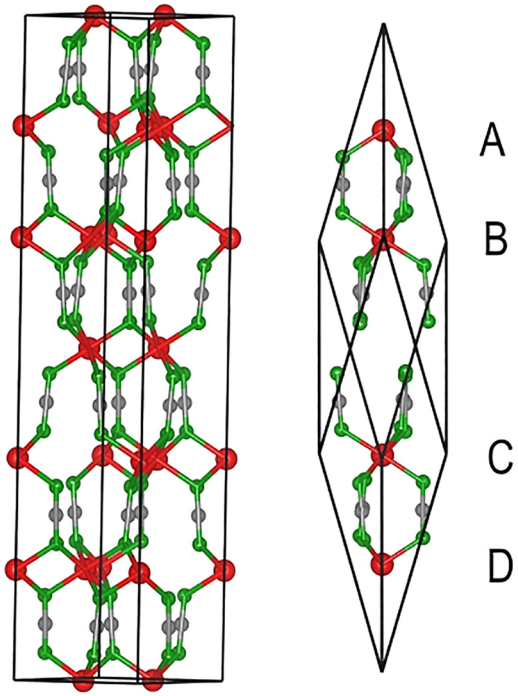

Figure 1: Crystal unit cell (left panel) and primitive trigonal unit cell (right panel) of $Fe_2(NCN)_3$ in which Fe, N, and C atoms are shown in red, green, and grey, respectively. The labels A, B, C, and D in the right panel refer to different magnetic orientations of the local metallic magnetic moment.

sum of the reactants, with the reaction referring to those used for $Cr_2(NCN)_3$ and MNCN compounds (M = Mn, Fe, Co, Ni) as shown in Eq. (1). For the reactants, the space groups of $FeCl_3$, ZnNCN, and $ZnCl_2$ are $R\bar{3}$, $I\bar{4}2d$, and $Pna2_1$, respectively.

$$2FeCl_3 + 3ZnNCN = Fe_2(NCN)_3 + 3ZnCl_2 \quad (1)$$

$$2Fe + 3C + 3N_2 = Fe_2(NCN)_3 \quad (2)$$

The calculated chemical reaction energy is –1.85 eV, indicating that the designed reaction is an attractive candidate. The formation enthalpy calculated from the direct route (Eq. (2)) starting with the elements Fe ($Im\bar{3}m$), C ($P6_3/mmc$) and N_2 ($P6_3/mmc$), is –18.85 eV, suggesting that $Fe_2(NCN)_3$ is thermodynamically stable relative to the elements.

Subsequently, we examined the mechanical stability of $Fe_2(NCN)_3$. The calculated elastic constants are $C_{11} = 174$, $C_{12} = 57$, $C_{13} = 128$, $C_{14} = 0$, $C_{33} = 567$, $C_{44} = 58$, and $C_{66} = 62$ GPa. For the rhombohedral *point group* $\bar{3}m$ structure, four necessary and sufficient conditions are required for elastic stability [38]:

$$\begin{cases} C_{11} > |C_{12}|\,;\, C_{44} > 0; \\ 2C_{13}^2 < C_{33}(C_{11} + C_{12}) \\ 2C_{14}^2 < C_{44}(C_{11} - C_{12}) \equiv C_{44}C_{66} \end{cases}$$

Obviously, $Fe_2(NCN)_3$ is mechanically stable because the calculated elastic stiffness constant C_{ij} satisfies the mechanical stability criteria of rhombohedral *point group* $\bar{3}m$ crystals. This is consistent with the experimental report that $Cr_2(NCN)_3$ in space group $R\bar{3}c$ is mechanically very stable [4].

To get a quantum-chemical insight into the conductivity and magnetic properties, we performed electronic structure calculations for $Fe_2(NCN)_3$. Besides the ferromagnetic (FM) structure with all the magnetic moments of Fe directing in the same direction, three additional antiferromagnetic structures were considered in which the four neighboring Fe^{3+} ions A, B, C, D along the [111] axis (Figure 1, right) have different orientations with respect to their local moments. If the symbols + and − represent a spin-up and spin-down orientation of a Fe moment, respectively, then the sequence ++++ stands for the FM (adopted by $Cr_2(NCN)_3$) [4], +−+− for AFM1 (adopted by Cr_2O_3) [39], ++−− for AFM2 (adopted by α-Fe_2O_3) [37], while +−−+ belongs to AFM3 (no representative to date).

In the GGA context, the FM state is the most stable one with the total energy lower than AFM1, AFM2, and AFM3 by 14, 56, and 64 meV per formula unit, respectively, as shown in Table 1. This is similar to the results for the isostructural ferromagnetic $Cr_2(NCN)_3$, but quite different from those for the isostructural AFM2 α-Fe_2O_3. The calculated spin saturation moment for the Fe ion is 0.93 μ_B in FM, and a little more than 1 μ_B in other antiferromagnetic phases, consistent with a $S = 1/2$ scenario. Obviously, the 3*d* orbitals of Fe^{3+} ions in the distorted FeN_6 octahedron are in the low-spin configuration, i.e. $t_{2g}^5 e_g^0$, in contrast to the high-spin occupation in AFM2 α-Fe_2O_3 [37] and in antiferromagntic MNCN compounds (M = Mn, Fe, Co, Ni) [2, 19, 20]. This low-spin state of the Fe^{3+} ion was observed in alkylperoxoiron(III) complexes with weak Fe–O bonds [40].

Generally, the electronic correlations (Coulomb interaction, *U*) are believed to be necessary to study the electronic and magnetic properties of 3*d* transition metal oxides, which have not been properly considered within the GGA. Therefore, calculations of the electronic structures of $Fe_2(NCN)_3$ were also performed using the GGA + *U* method in which *U* was set to a series of values, 1, 2, 3, and 4 eV, in order to investigate the correlation effect on the Fe^{3+} ions in low-spin occupation. The results are listed in Table 1. With a correlation *U* applied, AFM1 turns to be the most stable phase, and with *U* increasing to 4 eV, the total energy is lower than that of the other three magnetic phases by almost 2 eV per formula unit. In contrast, the FM phase changes from the most stable phase in $U = 0$ eV to the most unstable one as *U* is larger than 1 eV. It can be seen from Table 1 that the correlation, however, has very little influence on the spin saturation moment of the Fe^{3+} ions, which is quite different from the scenario in Fe^{3+}-based oxides [41]. Regarding the subtle changes, we can see that the spin saturation moment of the Fe ions in FM and AFM1 reach a maximum as *U* equals to 1 eV, but as *U* increases further, it decreases a little. Clearly, the electronic correlation probably has a very weak influence on the situation in $Fe_2(NCN)_3$ with Fe^{3+} ions in the low-spin state. Therefore, the electronic structures both in FM and AFM1 phases are discussed further in the following.

The local densities-of-states (DOS) within the FM states as derived from $U = 0$ and $U = 3$ eV are shown in Figure 2 (left panel). In the GGA description, the Fe–N orbital mixing is very weak. For the majority spin channel, an energy gap of 0.79 eV is clearly seen between the highest occupied valence bands with Fe t_{2g} character and the lowest-lying conduction bands of Fe e_g character, while for the minority spin channel, a metallic behavior is observed because the partially filled t_{2g} orbitals occupy the Fermi level. This suggests that $Fe_2(NCN)_3$ in FM shows a half-metallic behavior with Fe^{3+} in the low-spin state. With a correlation of $U = 3$ eV applied, the shape of the local DOS keeps similar to that of $U = 0$, but the energy gap in the majority spin channel increases to 1.32 eV.

Table 1: Calculated total energy E_{tot} (eV) per formula unit, magnetic moments, μ (μ_B) of Fe^{3+} ions of $Fe_2(NCN)_3$ in the FM, AFM1, AFM2, and AFM3 magnetic orderings based upon GGA and GGA + U calculations with U set as 1, 2, 3, and 4 eV.

		U = 0	U = 1 eV	U = 2 eV	U = 3 eV	U = 4 eV
E_{tot}, eV	FM	−91.7249	−89.8067	−87.9576	−86.1939	−84.5292
	AFM1	−91.7108	−89.9492	−88.4253	−87.0153	−85.6927
	AFM2	−91.6691	−89.7807	−88.0174	−86.3210	−84.6765
	AFM3	−91.6610	−89.7978	−88.0459	−86.3569	−84.7200
μ_{Fe}, μ_B	FM	0.93	0.94	0.93	0.92	0.88
	AFM1	±1.23	±1.30	±1.27	±1.24	±1.25
	AFM2	±1.13	±1.12;	±1.18	±1.26	±1.33
	AFM3	±1.11	±1.12	±1.19	±1.23	±1.05

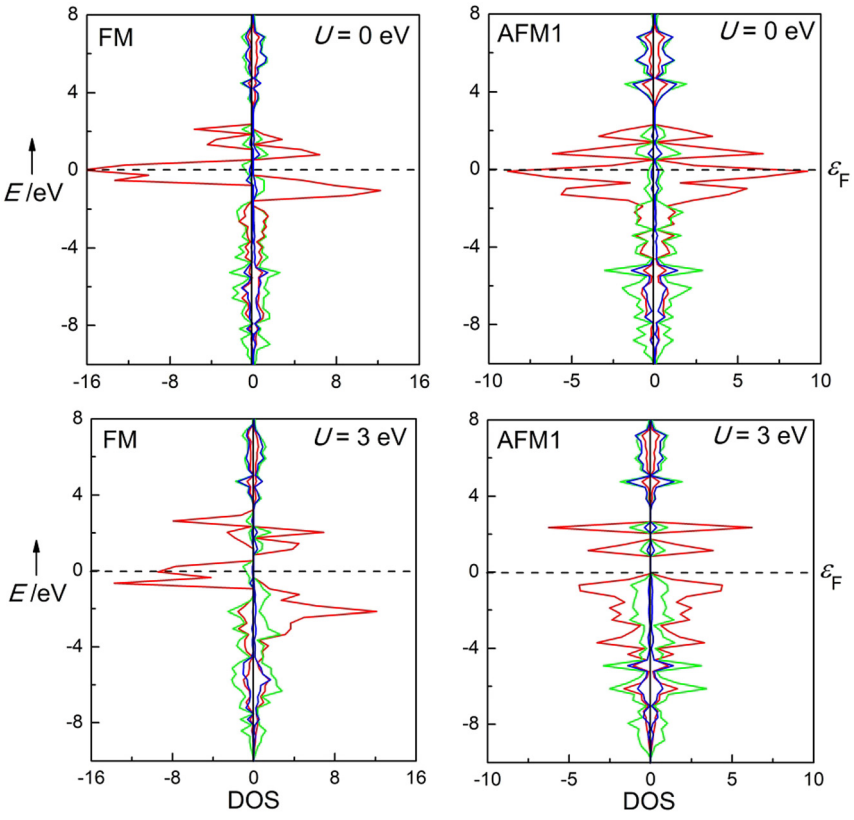

Figure 2: The local densities-of-states (DOS) of the Fe 3*d* (red), N 2*p* (green) and C 2*p* (blue) orbitals of $Fe_2(NCN)_3$ in the FM (left panel) and AFM1 (right panel) states as modeled from GGA (U = 0 eV) (upper row) and GGA + U (U = 3 eV) (lower row) calculations, with the spin-up and spin-down electrons given to the right and left in each frame. The energy zero indicates the Fermi level.

The local DOS of $Fe_2(NCN)_3$ in the AFM1 states calculated by U = 0 and U = 3 eV are shown in the right panel of Figure 2. For the uncorrelated U = 0 case, $Fe_2(NCN)_3$ in AFM1 is definitely metallic because there is a large DOS at the Fermi level. With the correlation U = 3 eV, the conduction bands are shifted to a higher energy region with respect to the valence band maximum. As a consequence, there results a band gap of 0.83 eV between the highest occupied valence bands (majority Fe t_{2g}) and the lowest-lying conduction bands (majority Fe e_g, minority Fe t_{2g}), thereby classifying $Fe_2(NCN)_3$ as a d–d Mott–Hubbard insulator.

Figure 3 shows the phonon dispersion curves of $Fe_2(NCN)_3$ in the FM and AFM1 states. For the AFM1 state, $Fe_2(NCN)_3$ has large imaginary modes and hence is dynamically unstable. However, with a ferromagnetic order allowed, it turns to be stable dynamically without the imaginary modes. Obviously, for $Fe_2(NCN)_3$ a ferromagnetic half-metallic property is preferred with the Fe^{3+} ions in a low-spin state.

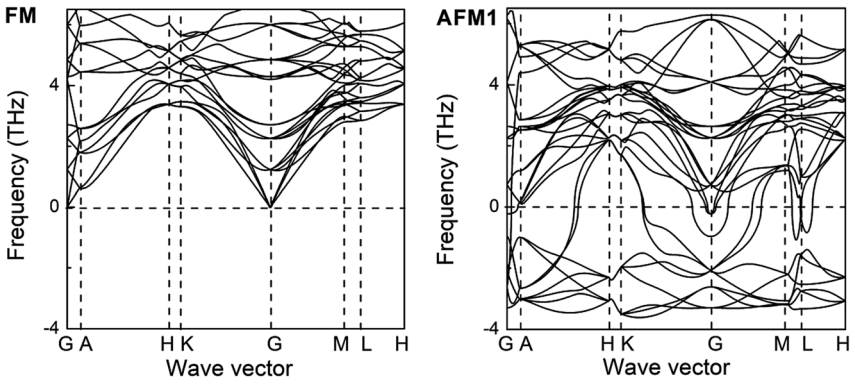

Figure 3: Calculated phonon dispersion relations of $Fe_2(NCN)_3$ in FM state (left panel) and AFM1 state (right panel). Imaginary phonon frequencies are shown by negative values.

4 Conclusions

We predict the existence and properties of the first low-spin 3*d* transition metal carbodiimide, $Fe_2(NCN)_3$, using density functional theory. $Fe_2(NCN)_3$ in space group $R\bar{3}c$ is stable both thermodynamically and mechanically. Four magnetic ordering variants were considered for $Fe_2(NCN)_3$ and the results show that $Fe_2(NCN)_3$ is most stable in a FM half-metallic state derived from GGA calculations, but turns to be most stable in AFM1 semiconducting state when including the electronic correlation (GGA + *U*). The calculated magnetic moments show that the Fe^{3+} ion in $Fe_2(NCN)_3$ is in the low-spin state, and the electronic correlation has only a minor influence on it. The phonon dispersion relations indicate that $Fe_2(NCN)_3$ is dynamically stable only in the FM state. Thus $Fe_2(NCN)_3$ in space group $R\bar{3}c$ is predicted to be a ferromagnetic half-metal. It would be an interesting compound as a spintronic material, and we wish it could be demonstrated in a future experimental study.

Author contributions: All the authors have accepted responsibility for the entire content of this submitted manuscript and approved submission.
Research funding: This work was supported by the National Natural Science Foundations of China (51971159).
Conflict of interest statement: The authors declare no conflicts of interest regarding this article.

References

1. Liu X., Krott M., Müller P., Hu C., Lueken H., Dronskowski R. *Inorg. Chem.* 2005, *44*, 3001–3003.
2. Krott M., Liu X., Fokwa B. P. T., Speldrich M., Lueken H., Dronskowski R. *Inorg. Chem.* 2007, *46*, 2204–2207.
3. Liu X., Wankeu M. A., Lueken H., Dronskowski R. *Z. Naturforsch.* 2005, *60b*, 593–596.
4. Tang X. J., Xiang H. P., Liu X. H., Speldrich M., Dronskowski R. *Angew. Chem. Int. Ed.* 2010, *49*, 4738–4742.
5. Jacobs P., Houben A., Senyshyn A., Müller P., Dronskowski R. *J. Solid State Chem.* 2013, *202*, 149–153.
6. Krott M., Houben A., Müller P., Schweika W., Dronskowski R. *Phys. Rev. B* 2009, *80*, 024117 (5 pages).
7. Liu X., Dronskowski R., Kremer R. K., Ahrens M., Lee C., Whangbo M.-H. *J. Phys. Chem. C* 2008, *112*, 11013–11017.
8. Jacobs P., Houben A., Tchougréeff A. L., Dronskowski R. *J. Chem. Phys.* 2013, *139*, 224707 (5 pages).
9. Xiang H. P., Dronskowski R., Eck B., Tchougréeff A. L. *J. Phys. Chem. A* 2010, *114*, 12345–12352.
10. Xiang H. P., Liu X. H., Dronskowski R. *J. Phys. Chem. C* 2009, *113*, 18891–18896.
11. Sougrati M. T., Darwiche A., Liu X., Mahmoud A., Hermann R. P., Jouen S., Monconduit L., Dronskowski R., Stievano L. *Angew. Chem.* 2016, *55*, 5090–5095.
12. Eguía-Barrio A., Castillo-Martínez E., Liu X., Dronskowski R., Armand M., Rojo T. *J. Mater. Chem. A* 2016, *4*, 1608–1611.
13. Eguía-Barrio A., Castillo-Martínez E., Klein F., Pinedo R., Lezama L., Janek J., Adelhelm P., Rojo T. *J. Power Sources* 2017, *367*, 130–137.
14. Sougrati M. T., Arayamparambil J. J., Liu X., Mann M., Slabon A., Stievano L., Dronskowski R. *Dalton Trans.* 2018, *47*, 10827–10832.
15. Eguía-Barrio A., Castillo-Martínez E., Liu X., Dronskowski R., Lezama L., Armand M., Rojo T. *MRS Adv.* 2017, *2*, 1165–1176.
16. Arayamparambil J. J., Mann M., Liu X., Alfredsson M., Dronskowski R., Stievano L., Sougrati M. T. *ACS Omega* 2019, *4*, 4339–4347.
17. Arayamparambil J. J., Chen K. X., Ladecola A., Mann M., Qiao X. J., Fraisse B., Dronskowski R., Stievano L., Sougrati M. T. *Energy Technol.* 2020, *8*, 1901260 (12 pages).
18. Schädler H.-D., Jäger L., Senf I. *Z. Anorg. Allg. Chem.* 1993, *619*, 1115–1120.
19. Liu X., Stork L., Speldrich M., Lueken H., Dronskowski R. *Chem. Eur. J.* 2009, *15*, 1558–1561.
20. Boyko T. D., Green R. J., Dronskowski R., Moewes A. *J. Phys. Chem. C* 2013, *117*, 12754–12761.
21. Tchougréeff A. L., Dronskowski R. *J. Phys. Chem. A* 2011, *115*, 4547–4552.
22. Sterri K. B., Besson C., Houben A., Jacobs P., Hoelzel M., Dronskowki R. *New. J. Chem.* 2016, *40*, 10512–10519.
23. Hohenberg P., Kohn W. *Phys. Rev. B* 1964, *136*, 864–871.
24. Kohn W., Sham L. J. *Phys. Rev.* 1965, *140*, A1133–A1138.

25. Kresse G., Hafner J. *Phys. Rev. B* 1993, *48*, 13115–13118.
26. Kresse G. *Phys. Rev. B* 1996, *54*, 11169–11186.
27. Kresse G., Furthmüller J. *Comput. Mater. Sci.* 1996, *6*, 15–50.
28. Perdew J. P., Burke K., Ernzerhof M. *Phys. Rev. Lett.* 1996, *77*, 3865–3868.
29. Blöchl P. E. *Phys. Rev. B* 1994, *50*, 17953–17979.
30. Kresse G., Joubert D. *Phys. Rev. B* 1999, *59*, 1758–1775.
31. Peter E., Jepsen O., Andersen O. K. *Phys. Rev. B* 1994, *49*, 16223–16233.
32. Anisimov V. I., Poteryaev A. I., Korotin M. A., Anokhin A. O., Kotliar G. *J. Phys. Condens. Matter* 1997, *9*, 7359–7367.
33. Dudarev S. L., Botton G. A., Savrasov S. Y., Humphreys C. J., Sutton A. P. *Phys. Rev. B* 1998, *57*, 1505–1509.
34. Giannozzi P., de Gironcoli S., Pavone P., Baroni S. *Phys. Rev. B* 1991, *43*, 7231–7242.
35. Gonze X., Lee C. *Phys. Rev. B* 1997, *55*, 10355–10368.
36. Togo A., Tanaka I. *Scr. Mater.* 2015, *108*, 1–5.
37. Shull C. G., Strauser W. A., Wollan E. O. *Phys. Rev.* 1951, *83*, 333–345.
38. Mouhat F., Coudert F.-X. *Phys. Rev. B* 2014, *90*, 224104 (4 pages).
39. McGuire T. R., Scott E. J., Grannis F. H. *Phys. Rev.* 1956, *102*, 1000–1003.
40. Krishnamurthy D., Kasper G. D., Namuswe F., Kerber W. D., Narducci Sarjeant A. A., Moënne-Loccoz P., Goldberg D. P. *J. Am. Chem. Soc.* 2006, *128*, 14222–14223.
41. Wang L., Maxisch T., Ceder G. *Phys. Rev. B* 2006, *73*, 195107 (6 pages).